SP17

Solidification Processing 2017

Proceedings of the
6th Decennial
International Conference on
Solidification Processing

25 - 28 July 2017
Beaumont Estate
Old Windsor, UK

Edited by Z. Fan

BCAST

Volume Average Modelling of Equiaxed-to-Columnar Transition in a Vertically Solidified Pb-18 wt.%Sn Cavity

Y. Zheng[1], M. Wu[1,2], A. Kharicha[1,2], A. Ludwig[1]

[1] Chair of Modelling and Simulation of Metallurgical Processes, Montanuniversitaet Leoben, Austria
[2] Christian Doppler Lab for Advanced Simulation of Solidification and Melting, Montanuniversitaet Leoben, Austria

Abstract

A detailed analysis is performed for the equiaxed-to-columnar transition (ECT) by a volume average numerical model. A special numerical benchmark was configured with Pb-18 wt.%Sn alloy. Geometry of 2D cavity (50 × 60 mm^2) with unidirectional cooling from the top boundary was considered. Modelling results show that the equiaxed crystals start to form from the top and fall down to the bottom. The settling equiaxed crystals pile up, and build a rigid crystal network at the bottom. Growth of the parked equiaxed crystals tends to develop columnar structure, but it is initially blocked by the oncoming equiaxed crystals from upper region. During the late stage of solidification, the inoculants are gradually consumed and no sufficient new equiaxed crystal forms in the upper region, and then the ECT occurs. Thereafter the rest domain of the benchmark solidifies as columnar structure.

Keywords: equiaxed-to-columnar transition (ECT), macrosegregation, simulation, Pb-Sn alloy.

1. Introduction

More attention has been paid to the CET (columnar-to-equiaxed transition) [1-3] than the ECT (equiaxed-to-columnar transition), although both phenomena are equally important in the formation of as-cast structure. When the bulk melt is intensively undercooled, solidification starts favourably as equiaxed crystals. This situation is common for the surface part of a solidifying ingot [4, 5], as shown in Fig. 1. When the initially-formed equiaxed crystals sediment in the casting bottom and no further equiaxed crystals is supplied, e.g. exhaust of inoculants, columnar would grow from the as-packed equiaxed crystals. Thus, the growth of columnar will overweigh that of the equiaxed during the late stage of solidification [6, 7]. Either CET or ECT is the result of growth competition between columnar and equiaxed structures, even under some circumstance they coexist. Studies on CET were carried to improve understanding of the blocking mechanism of the columnar growth by the equiaxed crystals [1, 8, 9]. With the CAFE (cellular automat and finite element) method the ECT including the globular/dendritic morphological transition can be naturally considered [10-12]. With the volume average method a special treatment is necessarily made for the ECT [6, 7, 13].

Mechanisms for the origin of equiaxed crystals, considering the transport phenomenon of inoculants and equiaxed crystals [7, 14, 15], are not fully understood. Heterogeneous nucleation as function of undercooling according to a Gaussian distribution law was usually assumed [16]. In this study, we use a volume average method to investigate the solidification process by considering the origin of the equiaxed crystals with the heterogeneous nucleation, transport of both inoculants and equiaxed crystals, and formation of as-cast structure with the ECT.

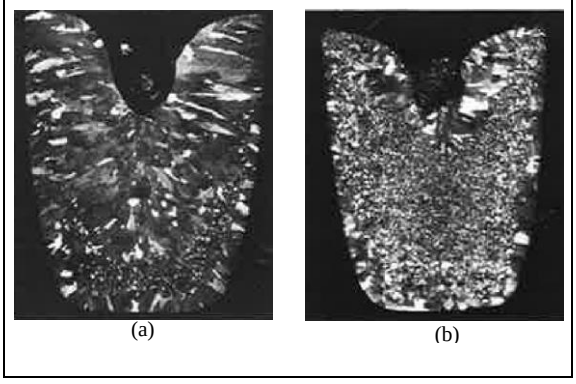

Figure 1: Examples of as-cast structures of Al-0.2%Cu (a) and Al-0.3%Be (b) ingots [5].

2. Numerical settings

A volume-average numerical model considering ECT was recently proposed by the authors [6, 7] and it is used here to investigate the equiaxed-to-columnar transition (ECT). The densities for both solid and liquid phases are assumed equal and solidification shrinkage is ignored, but the thermo-solutal convection and crystals sedimentation is modelled with a Boussinesq approximation. The solidified equiaxed crystals sink due to gravity. Nucleation of equiaxed crystals occurs according to a classical heterogeneous nucleation law. The inoculants serve as nucleation sites, which are activated as equiaxed nuclei by undercooling:

$$N_{nu} = \frac{D(\Delta T)}{Dt} \cdot \frac{dn_{eq}}{d(\Delta T)} \quad (1)$$

$$\frac{D(\Delta T)}{Dt} = \frac{\partial T}{\partial t} + u_\ell \cdot (m \cdot \frac{\partial c_\ell}{\partial x} - \frac{\partial T_\ell}{\partial x}) + v_\ell \cdot (m \cdot \frac{\partial c_\ell}{\partial y} - \frac{\partial T_\ell}{\partial y}) \quad (2)$$

$$\frac{dn_{eq}}{d(\Delta T)} = \frac{n_{em}}{\sqrt{2\pi} \cdot \Delta T_\sigma} \cdot e^{-\frac{1}{2}\left(\frac{\Delta T - \Delta T_N}{\Delta T_\sigma}\right)^2} \quad (3)$$

The transports of equiaxed inoculants (n_{em}) and crystals (n_{eq}), as well as their conservation are calculated as follows:

$$\frac{\partial}{\partial t} n_{em} + \nabla \cdot (\vec{u}_\ell n_{em}) = -N_{nu} \quad (4)$$

$$\frac{\partial}{\partial t} n_{eq} + \nabla \cdot (\vec{u}_e n_{eq}) = N_{nu} \quad (5)$$

When the equiaxed crystals are arrested by any obstacle, e.g. the mould wall, columnar structure develops from the stationary equiaxed crystals. Additionally, the equiaxed-to-columnar transition (ECT) occurs when no sufficient equiaxed crystals ahead of the columnar tip front blocks the growth of columnar dendrite tips [2]. The ECT model used in this study is integrated in a three-phase mixed columnar-equiaxed solidification model, which can be found in the literature [9]. The equiaxed morphology and interdendritic flow is taken into account [17]. The present model is conducted within the framework of the CFD software ANSYS-Fluent version 14.5. Two quantities are defined to analyse the macrosegregation: the mixture concentration, $c_{mix} = (c_\ell \rho_\ell f_\ell + c_c \rho_c f_c + c_e \rho_e f_e)/(\rho_\ell f_\ell + \rho_c f_c + \rho_e f_e)$, and the segregation index, $c^{index} = (c_{mix} - c_0) \times 100 / c_0$.

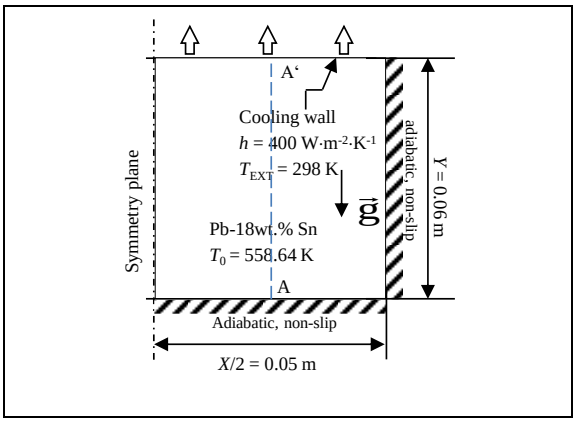

Figure 2: Benchmark geometry with boundary and initial conditions.

The geometry, boundary conditions and initial conditions are shown in Fig. 2. The heat is continuously extracted from the top of the cavity, and solidification starts there. Gravity is always downward, and the equiaxed phase tends to settle down. Pb-18 wt.%Sn alloy is chosen as the model material. Thermal and physical parameters of Pb-18 wt.%Sn alloys are listed in Tab. 1.

Table 1: Material properties and other parameters.

Parameters	Sym.	Units	Value	Ref.
Nominal comp.	c_0	1	0.18	
Liquidus temp.	T_{liq}	K	558.63	[18]
Melting point of solvent at $c_0 = 0$	T_m	K	600.65	[18]
Eutectic comp.	c_e	1	0.619	[18]
Eutectic temp.	T_e	K	456	[19]
Liquidus slope	m	K/wt.%	-233.4	[18]
Equilibrium partition coeff.	k	1	0.310	[18]
Reference density	ρ_{ref}	kg·m^{-3}	9250	[18]
Specific heat	c_p^ℓ, c_p^s	J kg^{-1} K^{-1}	176	[18]
Thermal cond.	k_ℓ, k_s	W m^{-1} K^{-1}	17.9	[18]
Latent heat	Δh_f	J kg^{-1}	3.76 × 10^4	[18]
Viscosity	μ_ℓ	Kg m^{-1} s^{-1}	1.1 × 10^{-3}	[18]
Liquid thermal expansion coeff.	β_T	K^{-1}	1.16 ×10^{-4}	[18]
Liquid solutal expansion coeff.	β_C	wt.%$^{-1}$	4.9 × 10^{-3}	[18]
Primary dendritic arm spacing	λ_1	m	1.85 × 10^{-3}	[18]
Second dendritic arm spacing	λ_2	m	1.85 × 10^{-4}	[18]
Diffusion coeff. (liquid)	D_ℓ	m^2 s^{-1}	4.5 × 10^{-9}	[20]
Initial temp.	T_0=T_{liq}	K	558.64	[18]
Heat transfer coeff.	h	W m^{-2} K^{-1}	400	[18]
External temp.	T_{EXT}	K	298	[18]
Solid-liquid density difference	$\Delta\rho$	kg m^{-3}	420	[21]
Gibbs Thomson coeff.	Γ	m K	7.9 × 10^{-8}	[22]
Initial inoculant number density	n_{em}^0	m^{-3}	1.0 × 10^{10}	
Initial equiaxed number density	n_{eq}^0	m^{-3}	1.0 × 10^7	
Gaussian distribution width	ΔT_N	K	3.0	
Undercooling for maximum grain production rate	ΔT_σ	K	5.0	

3. Results

3.1 Solidification process with ECT

The solidification sequence of the benchmark considering ECT is shown in Fig. 3. Nucleation (Fig. 3 c.x) and solidification start from the top surface. The sinking

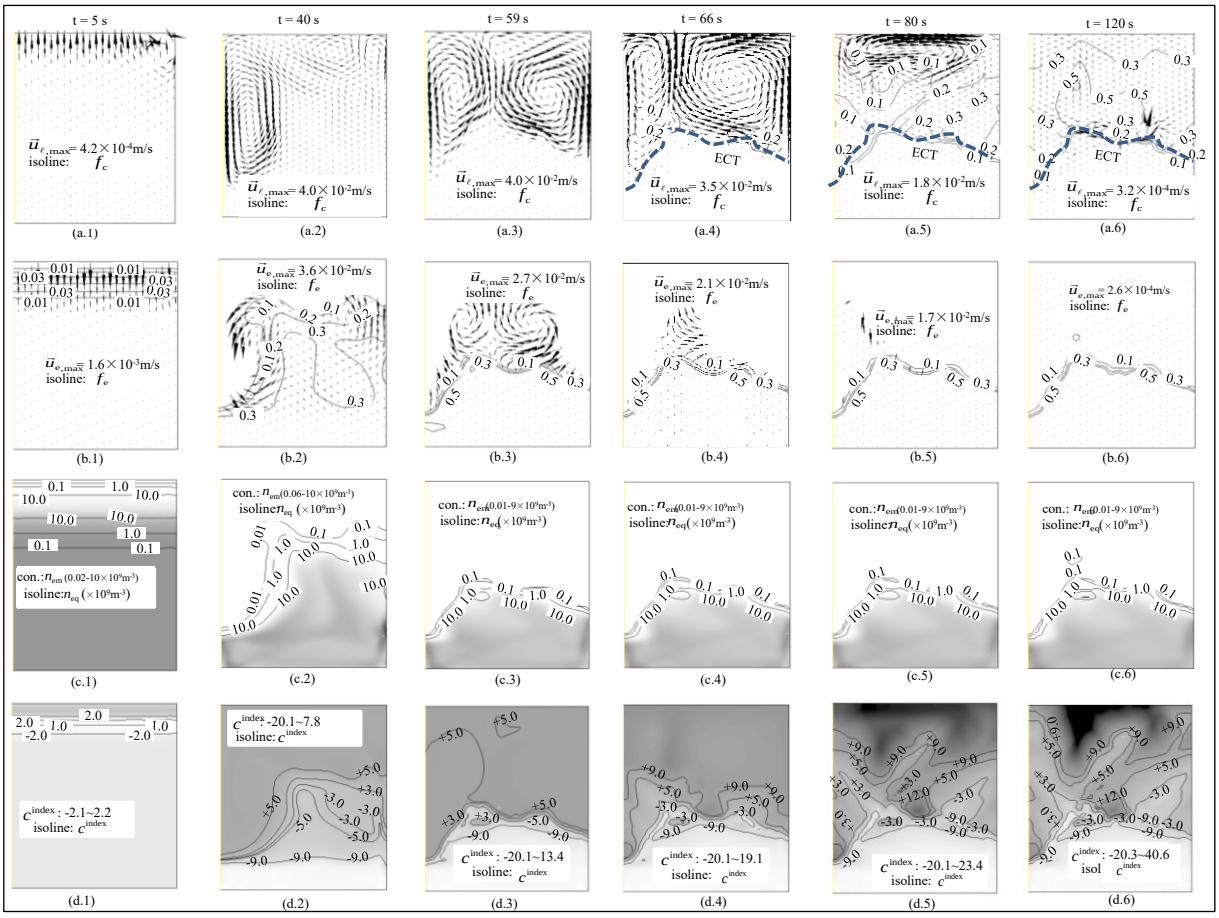

Figure 3: Solidification sequence: a.x shows the liquid velocity overlaid by f_e isolines, as well as the ECT (dash line in a.4-a.6); b.x shows the equiaxed velocity overlaid by f_e isolines; c.x shows the evolution of n_{em} in grey scale overlaid by n_{eq} isolines; d.x shows the evolution of macrosegregation index overlaid by its isolines.

equiaxed grains together with the thermos-solutal convection of the melt (Fig. 3 b.x) introduce a transient melt flow in the bulk (Fig. 3 a.x). The nucleation of equiaxed crystals occurs in the upper part, consuming the inoculants. The liquid flow, however, has the ability to bring more inoculants from the bottom region back to the upper region. Those inoculants can be activated and transferred into equiaxed nuclei by the undercooling according to Eq. (1)-(3), then the newly born equiaxed crystals would grow and settle down to the lower part. Actually, this kind of transport and activation of the inoculants as equiaxed grains exist universally from the beginning of the solidification till the consumption of all inoculants. Thus advection of the inoculants is very important to the final structure distribution and macrosegregation. Equiaxed grains sink and further pile-up at the bottom. For the present case, most of the inoculants are consumed at about 60 s and ECT occurs then. Afterwards, the columnar phase grows very fast into the undercooled liquid region till it reaches the top of the benchmark (Fig. 3 (a.3)-(a.6)). Consequently, a rigid network would form all over the domain. Due to the consistent temperature gradient from the top to bottom, the solidification sequence in the columnar structure develops even reversely downwards. This kind of process forms the general distribution pattern of macrosegregation. The total solidification process lasts 550 s. Fig. 3 d.x show the evolution of macrosegregation. A sedimentation-induced negative macrosegregation at the bottom region and a positive macrosegregation in the top are obtained.

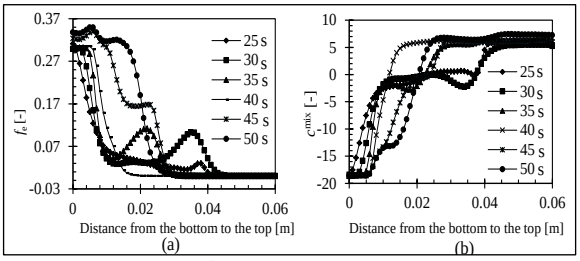

Figure 4: Evolution of f_e (a) and macrosegregation index (b) along the vertical line (A-A' in Fig. 2) of solidifying benchmark from 25 s to 50 s.

Sedimentation of equiaxed phase leads to the accumulation of equiaxed in the bottom of the benchmark. Fig. 4 shows the evolution of f_e and macrosegregation index along a vertical line in the solidifying benchmark from 25 s to 50 s. As solidification proceeds, the settling of equiaxed phase makes the region of compact equiaxed phase extend gradually (Fig. 4(a)). Accordingly, the 'S' shape of c^{index} curves moves upwards (Fig. 4(b)). This sedimentation phenomenon continues till all the inoculants are mostly consumed. Afterwards, the equiaxed region will not change in the further solidification and the columnar structure growth will dominant the

solidification of late stage, resulting in equiaxed-columnar-transformation (ECT).

The final simulation results (550 s) are shown in Fig. 5. Lower part of the benchmark has negative macrosegregation while the upper part has positive segregation (Fig. 5(a)). The range of c^{index} is from -32.1 to 46.8. As-cast structure contains an equiaxed zone taking about 1/3 height of the benchmark in the lower part and the rest is occupied by columnar phase. They are separated by a ECT line (Fig. 5(b)-(c)).

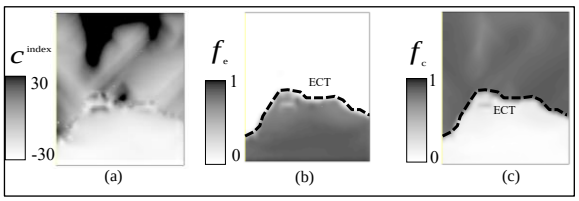

Figure 5: Final simulation results (550 s) of as-solidified benchmark: (a) macrosegregation index; (b) volume fraction of equiaxed phase; (c) volume fraction of columnar phase.

3.2 Solidification without ECT

In order to demonstrate the importance of ECT, an additional case without considering ECT in the model is simulated. It means that the model has 'switched off' the functionality of ECT. The simulation result for the moment at 550 s is shown in Fig. 6. Normally, solidification should finish at this moment, but it does not. The rest of the domain is still filled with liquid although its temperature falls below the eutectic point (Fig. 6(b)). The reason is that all of the inoculants are consumed in the rest melt and no new equiaxed crystal would appear, and in the meantime ECT event is 'switched off' by the numerical model, hence no columnar can develop. Therefore, the rest melt remains as liquid state. This phenomenon is not feasible in the real solidification process, since columnar phase would have grown into the undercooling melt and the solidification would continue until all rest melt is consumed.

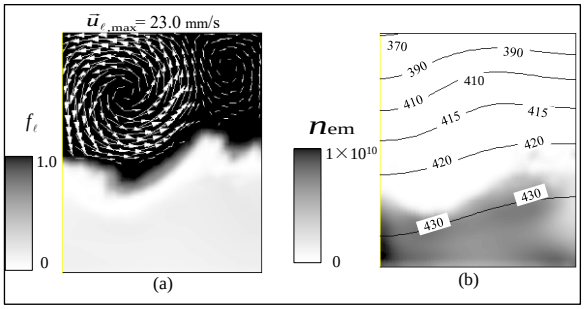

Figure 6: Simulation result for the moment at 550 s without considering ECT: (a) liquid fraction overlaid with liquid velocity; (b) contour of number density of inoculants overlaid with temperature isolines in Kalvin.

4. Conclusions

A modified three-phase volume average model considering ECT is used to investigate the solidification process of Pb-18wt.%Sn benchmark. Calculations of the transport of inoculants (nucleus embryos), nucleation, transport and growth of equiaxed crystals, equiaxed-to-columnar transit (ECT), formation of macrosegregation and as-cast structure are made. The columnar phase is allowed to grow when the equiaxed phase is impinged with each other and f_e exceeds the packing limit. During the early stage of solidification the growth of equiaxed phase overweighs that of columnar phase. When the inoculants are mostly consumed during the late stage of solidification, columnar phase will grow into the undercooling bulk liquid till most of the liquid transfers into solid phase, resulting in equiaxed-to-columnar transit (ECT).

If the ECT mechanism is not included in the volume average model, the Pb-18 wt.%Sn melt with presumed n_{em} = 1.0×10^{10} m^{-3} cannot fully solidify when the inoculants are consumed, even though it is considerably undercooled. Therefore, it is absolutely necessary to include the ECT into consideration in the volume average model.

Acknowledgements

The authors acknowledge the financial support from Austrian Research Promotion Agency (FFG) through the project of Bridge Early Stage (No. 842441), as well as the technical support of the industrial partner Primetals (former Siemens VAI).

References

1. J. Hunt, *Mater. Sci. Eng.*, 1984, 65: 75.
2. M. Martorano, C. Beckermann, C.-A. Gandin, Metall. *Mater. Trans. A*, 2003, 34: 1657.
3. M. Wu, A. Ludwig, *Metall. Mater. Trans. A*, 2007, 38A: 1465.
4. W. Kurz, D.J. Fisher, *Fundamentals of solidification*, *Trans Tech Publications*, 1984.
5. A. Ohno, *Solidification: the Separation Theory and Its Practical Applications*, Springer-Verlag, 1987.
6. M. Wu, Y. Zheng, A. Kharicha, A. Ludwig, *Comp. Mater. Sci.*, 2016, 124: 444.
7. Y. Zheng, M. Wu, A. Kharicha, A. Ludwig, *Comp. Mater. Sci.*, 2016, 124: 456.
8. M. Martorano, V. Biscuola, *Acta Mater.*, 2009, 57: 607.
9. M. Wu, A. Ludwig, Metall. *Mater. Trans. A*, 2006, 37A: 1613.
10. B. Šarler, A.Z. Lorbiecka, *Mater. Sci. Forum.*, 2010, 649: 373.
11. B. Appolaire, H. Combeau, G. Lesoult, *Mater. Sci. Eng. A*, 2008, 487: 33.
12. G. Guillemot, C.-A. Gandin, H. Combeau, *ISIJ Int.*, 2006, 46: 880.
13. N. Leriche, H. Combeau, C.-A. Gandin, M. Založnik, *IOP Conf. Series: Mate. Sci. Eng.*, 2015, 84: 012087.
14. M. Bedel, K. Tveito, M. Založnik, H. Combeau, M. M'Hamdi, *Comp. Mater. Sci.*, 2015, 102: 95.
15. M. Bedel, M. Založnik, A. Kumar, H. Combeau, P. Jarry, E. Waz, *IOP Conf. Series: Mate. Sci. Eng.*, 2012, 27: 012070.
16. M. Rappaz, *Int. Mater. Rev.*, 1989, 34: 93.
17. M. Wu, A. Ludwig, *Acta Mater.*, 2009, 57: 5621.
18. M. Bellet, H. Combeau, Y. Fautrelle, D. Gobin, M. Rady, E. Arquis, O. Budenkova, B. Dussoubs, Y. Duterrail, A. Kumar, *Int. J. Therm. Sci.*, 2009, 48: 2013.

19. N. Ahmad, J. Rappaz, J.-L. Desbiolles, T. Jalanti, M. Rappaz, H. Combeau, G. Lesoult, C. Stomp, *Metall. Mater. Trans. A*, 1998, 29: 617.
20. M. Klassen, J. Cahoon, *Metall. Mater. Trans. A*, 2000, 31: 1343.
21. O.L. Rocha, C.A. Siqueira, A. Garcia, *Metall. Mater. Trans. A*, 2003, 34: 995.
22. E. Cadirli, M. Gündüz, *J. Mater. Sci.*, 2000, 35: 3837.